Letter | Editors' Suggestion

Quantum Mpemba effect without global symmetries

Tanmay Bhore,[1] Lei Su,[2] Ivar Martin,[3,2] Aashish A. Clerk,[4] and Zlatko Papić[1]
[1]*School of Physics and Astronomy, University of Leeds, Leeds LS2 9JT, United Kingdom*
[2]*Department of Physics, University of Chicago, Chicago, Illinois 60637, USA*
[3]*Materials Science Division, Argonne National Laboratory, Lemont, Illinois 60439, USA*
[4]*Pritzker School of Molecular Engineering, University of Chicago, Chicago, Illinois 60637, USA*

(Received 28 May 2025; accepted 21 August 2025; published 26 September 2025)

The Mpemba effect, where a system initially farther from equilibrium relaxes faster than one closer to equilibrium, has been extensively studied in classical systems and recently explored in quantum settings. While previous studies of the quantum Mpemba effect (QME) have largely focused on isolated systems with global symmetries, we argue that the QME is ubiquitous in generic, nonintegrable many-body systems lacking such symmetries, including U(1) charge conservation, spatial symmetries, and even energy conservation. Using paradigmatic models such as the quantum Ising model with transverse and longitudinal fields, we show that the QME can be understood through the energy density of initial states and their inverse participation ratio in the energy eigenbasis. Our findings provide a unified framework for the QME, linking it with classical thermal relaxation.

DOI: 10.1103/1td3-2vwf

Introduction. The approach to thermal equilibrium is the ultimate fate of most interacting systems in nature, both classical and quantum. The rate at which this happens, however, can vary wildly depending on the initial microscopic configurations and the nature of interactions. A celebrated example, dating back to antiquity and systematically studied since the 1960s, is the classical Mpemba effect [1]: the counterintuitive observation that a hot liquid can freeze faster than a colder liquid under certain conditions. While similar anomalous relaxation behaviors have been found in a variety of classical systems [2–6], the understanding of their origin remains an active area of research [7–11].

In contrast, quantum counterparts of the Mpemba effect have only recently garnered attention [12]. Much like its classical analog, the quantum Mpemba effect (QME) can be defined as an anomalous dynamical process where a system, initially farther from equilibrium, relaxes faster than a system that starts closer to equilibrium. In open quantum systems, the QME can be engineered by suppressing the slowest eigenmode of the Liouvillean [13,14], reminiscent of classical Markovian systems [4,8]. A variety of other mechanisms have also been recently explored [15–36]. Quantum simulations of the QME in the presence of Markovian dynamics have been performed with trapped ions [14,37] and superconducting qubits [38].

In this work we instead focus on *closed* quantum systems evolving under unitary dynamics. For such systems the QME can be conveniently probed by a global quantum quench: the system is prepared in a pure state—one that is not an eigenstate of the Hamiltonian—and then evolved under the Schrödinger equation. In this setting the process of equilibration is understood at the level of subsystems approaching the Gibbs ensemble at late times [39–41]. Signatures of the QME have been found in many examples of closed quantum systems, e.g., various types of spin models [42–44], free fermions and bosons [45,46], quantum circuits [47–53], many-body localized systems [54], and trapped ion experiments [55]. In particular, for integrable models, Ref. [56] developed a comprehensive understanding of the QME based on the quasiparticle picture of the spreading of correlations following the quench [57]. Nevertheless, these studies have mainly focused on a restricted class of models possessing a global U(1) symmetry, such as the conservation of particle number or spin magnetization. This raises a fundamental question: Is the QME possible in the absence of global symmetries?

In this paper we give an affirmative answer to the previous question by demonstrating that the QME can occur in generic many-body systems that are nonintegrable and lack global symmetries, such as U(1) charge, spatial symmetries, or even energy conservation. We consider the paradigmatic quantum Ising model in the presence of transverse and longitudinal fields, in both its Hamiltonian and Floquet incarnations, as well as local spin-chain models with random couplings. In all cases we show that the QME can be succinctly explained by taking into account (i) the energy density of the initial states, playing the role of effective temperature and (ii) the inverse participation ratio of the initial states in the energy eigenbasis. Our results point to the ubiquity of the QME in generic chaotic systems and provide a unified description that highlights the role of energy distributions.

Mixed-field Ising model. As our first example, we consider the one-dimensional mixed-field Ising model,

$$H^{\mathrm{MFIM}} = J_{zz}\sum_{i=1}^{N-1}\sigma_i^z\sigma_{i+1}^z + h_x\sum_{i=1}^{N}\sigma_i^x + h_z\sum_{i=2}^{N-1}\sigma_i^z, \quad (1)$$

Published by the American Physical Society under the terms of the Creative Commons Attribution 4.0 International license. Further distribution of this work must maintain attribution to the author(s) and the published article's title, journal citation, and DOI.

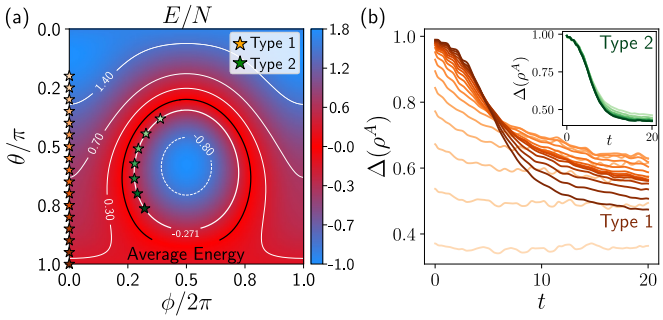

FIG. 1. QME in the mixed field Ising model, Eq. (1). (a) Energy density of tilted ferromagnetic states in Eq. (2) as a function of angles θ, ϕ, with isothermal levels marked by the contours. States with increasing energy (Type 1) and states at the same temperature (Type 2) are marked by the orange and green stars, respectively. As a guide to the eye, we also indicated the average energy (black curve). (b) Dynamics of trace distance, Eq. (3), for the subsystem density matrix ρ^A following the quench from Type 1 initial states, with Type 2 states shown in the inset. The lines correspond to the star symbols in panel (a). The QME is visible for states of Type 1 but it is absent for states of Type 2. Results are for system size $N = 14$ obtained by exact diagonalization. The subsystem A is chosen to be one half of the chain.

where $\sigma_j^{x,z}$ denote standard Pauli matrices on jth site and h_x, h_z are the transverse and longitudinal fields, respectively. We assume an open chain and include boundary fields, $\delta h_1^z = 0.25$ and $\delta h_N^z = -0.25$, to break reflection symmetry. The Hamiltonian (1) then lacks any symmetries except energy conservation. We fix the coupling strengths to $(J_{zz}, h_z, h_x) = (1, (1+\sqrt{5})/4, (\sqrt{5}+5)/8)$, for which the model is chaotic and shows ballistic growth of entanglement and diffusive energy transport [58], although we expect the results described here to hold for generic parameter choices for which the model is chaotic.

To reveal the QME, we consider translation-invariant product states:

$$|\theta,\phi\rangle = \bigotimes_{i=1}^{N} [\cos(\theta/2)|\uparrow\rangle_i + e^{i\phi}\sin(\theta/2)|\downarrow\rangle_i], \qquad (2)$$

where each spin points at the same angle (θ,ϕ) on the Bloch sphere. In isolated systems energy is conserved, hence we can assign a temperature to a state $|\Psi\rangle$ via its energy, $E_\Psi = \langle\Psi|H|\Psi\rangle = \frac{1}{\mathcal{Z}}\mathrm{Tr}(He^{-\beta H})$, where $\beta = 1/T$ is the inverse temperature in units $k_B = 1$ and $\mathcal{Z} = \mathrm{Tr}(e^{-\beta H})$. Infinite temperature or $\beta = 0$ corresponds to a uniform average of the eigenenergies, while energies away from the middle of the spectrum correspond to $\beta \neq 0$, i.e., finite (either positive or negative) temperatures.

The energy density of $|\theta,\phi\rangle$ states admits a simple form [59], which we plot as a function of (θ,ϕ) in Fig. 1(a). The color scale marks the effective temperature of the states; energies close to the edges of the spectrum are depicted in blue color, corresponding to low (positive or negative) temperatures, while the temperature progressively rises towards the middle of the spectrum, with the average energy corresponding to infinite temperature (red color). Among the states in Eq. (2), we consider two special types. Type 1 denotes ferromagnetic states with $\phi = 0$ that are rotated around the y axis, which progressively decreases their energy density. States of Type 2 are initial states degenerate in energy and away from the middle of the spectrum, thus at a fixed finite temperature.

Next, in Fig. 1(b) we quench the system from Type 1 and 2 initial states and monitor the evolution of trace distance [14,37] as a diagnostic of the QME:

$$\Delta(\rho^A)(t) = \tfrac{1}{2}||\rho^A(t) - \rho_{\mathrm{DE}}(\rho^A)||_1. \qquad (3)$$

Here $\rho^A = \mathrm{Tr}_B[\rho(t)]$ denotes the reduced density matrix for the bipartition of the system into two halves A and B, $\rho_{\mathrm{DE}}(\rho^A) = \sum_E \langle E|\rho(0)|E\rangle \mathrm{Tr}_B(|E\rangle\langle E|)$ is the diagonal ensemble [60] for the initial state $\rho(0)$, restricted to A via partial trace, and $|E\rangle$ are the energy eigenstates. The partial trace is required in Eq. (3) as the full state of the system—assumed to be pure initially—cannot evolve to a mixed state under unitary dynamics otherwise. Note that many previous studies used a different diagnostic of the QME, the "entanglement asymmetry" [12,42,61], but we employ a more general metric that does not rely on the presence of any global symmetry. In the Supplemental Material (SM) [59] we show that $\Delta(\rho^A)$ is a good diagnostic of the QME for U(1)-conserving systems, along with other measures, such as the Frobenius distance [12], which yield qualitatively similar conclusions.

For small tilt angles θ, Type 1 states are close to the edge of the spectrum and show almost no dynamics in Fig. 1(b). Upon increasing θ, the initial trace distance progressively increases, along with its rate of decay. This eventually leads to a crossing between successive states around $t \approx 4$ in Fig. 1(b). This is a manifestation of the QME, wherein hotter states relax to equilibrium faster than colder states. Note that in a chaotic system, $\Delta(\rho^A)(t \to \infty)$ is expected to approach 0 for the initial state at a finite energy density as the system size $N \to \infty$. The deviation seen in Fig. 1(b) is attributed to a finite-size effect; we perform a system-size scaling in the SM [59]. At the same time, we observe that the states of Type 2, which are degenerate in average energy, show little variation in their trace distance dynamics, with essentially identical initial trace distance and decay rates [inset of Fig. 1(b)]. This is consistent with the classical intuition where the Mpemba effect requires two initial states at different temperatures.

The role of energy distributions. In integrable systems, the QME arises due to states that are simultaneously more out-of-equilibrium and have larger overlaps with the fastest quasiparticle modes [56]. Similar mechanisms have been used to explain the effect in systems coupled to external reservoirs [62,63]. However, our model (1) is chaotic and lacks a quasiparticle description at high energies. In the absence of such a description, we instead look at the eigenstates themselves to understand the conditions for the QME.

Consider our initial pure state $|\Psi\rangle \equiv |\theta,\phi\rangle$. In the energy eigenbasis, the time-evolved density matrix can be decomposed into off-diagonal and diagonal components:

$$|\Psi(t)\rangle\langle\Psi(t)| = \rho_{\mathrm{DE}} + \sum_{n\neq m} c_n c_m^* e^{-i(E_n - E_m)t}|E_n\rangle\langle E_m|, \qquad (4)$$

where ρ_{DE} is the diagonal ensemble and $c_n = \langle E_n|\Psi\rangle$ encodes the energy overlaps of the initial state. Partial tracing both

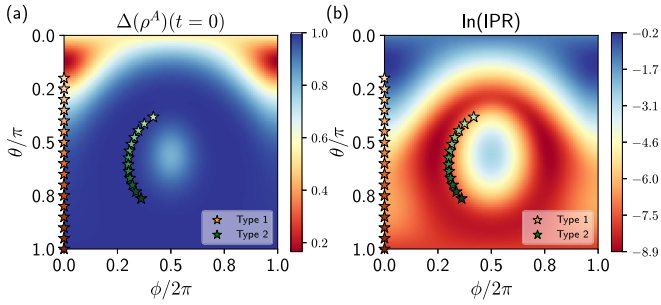

FIG. 2. Origin of the QME in the mixed field Ising model, Eq. (1). (a) Initial trace distance from the diagonal ensemble and (b) logarithm of the inverse participation ratio (IPR) of $|(\theta,\phi)\rangle$ states, Eq. (2). IPR anticorrelates with the initial trace distance: states with smaller IPR have larger initial trace distances and vice versa. Results are for $N = 14$.

sides to restrict to a subsystem, we get

$$\Delta(\rho^A)(t) = \frac{1}{2}\left|\left|\sum_{n\neq m} c_n c_m^* e^{-i(E_n-E_m)t}\mathrm{Tr}_B(|E_n\rangle\langle E_m|)\right|\right|_1. \quad (5)$$

The QME requires two conditions to be met: two states should have unequal initial trace distances, and the state with the larger initial trace distance must relax to thermal equilibrium faster than the other state. By Eq. (5), the trace distance at $t = 0$ is equal to $1/2||\sum_{m\neq n} c_n c_m^* \mathrm{Tr}_B(|E_n\rangle\langle E_m|)||_1$, which is a sum over $O(\mathcal{D}^2)$ eigenstate pairs, each weighed by the off-diagonal energy overlaps, where $\mathcal{D}$ denotes the Hilbert space dimension. If the initial state is an eigenstate, $\Delta(\rho^A)$ remains constant at all times and dynamics is frozen. If the initial state involves more eigenstates, a larger number of overlaps c_n contribute to the sum, which can lead to a larger initial trace distance. At the same time, a larger energy spread implies that a wider range of frequencies $E_n - E_m$ enter the exponent in Eq. (5), leading to faster dephasing and eventual thermalization. We expect this dephasing process to be the fastest at infinite temperature, wherein an $O(\mathcal{D}^2)$ frequencies enter the exponent.

Delocalization in the energy eigenbasis can then correlate with both conditions required for the QME. A simple quantity that quantifies this delocalization is the inverse participation ratio (IPR) [64],

$$\mathrm{IPR}(|\Psi\rangle) = \sum_E |\langle E|\Psi\rangle|^4, \quad (6)$$

where we assumed the state $|\Psi\rangle$ is normalized. The IPR takes values between $[1/\mathcal{D}, 1]$, where the limits correspond to a fully delocalized state (infinite temperature) and a single energy eigenstate, respectively. Since smaller IPR values correspond to more delocalized states, we expect an anticorrelation between IPR values and the initial trace distance, along with the speed of its decay.

We plot the initial trace distance $\Delta(\rho^A)(t = 0)$ and the logarithm of IPR for $|\theta,\phi\rangle$ states in Figs. 2(a) and 2(b). We observe a clear anticorrelation between the two, with regions corresponding to low IPR values showing large initial trace distances and vice versa. In particular, this explains the trace

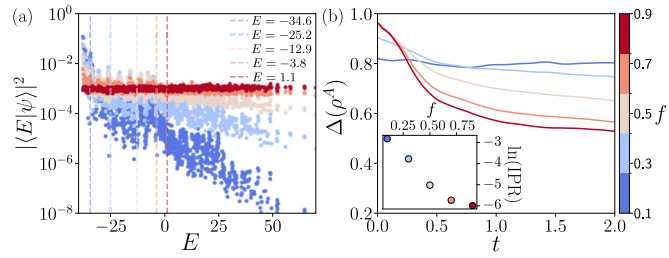

FIG. 3. QME in the random model, Eq. (7). (a) Overlap of $|(\theta_i,\phi_i)\rangle$ states with energy eigenstates as a function of their energy. The overlaps are averaged over 100 realizations of the angles. Different colors represent different values of f (see text), resulting in average energies given in the legend. (b) Trace distance dynamics for $|(\theta_i,\phi_i)\rangle$ states. The crossing associated with the QME is visible as the effective temperature of the state is tuned. The inset shows the IPR for the same states as a function of f. All data are for system size $N = 10$ and fixed disorder window $W = 1$.

distance dynamics observed in Fig. 1. The initial $\Delta(\rho^A)$ for Type 1 states increases while the IPR monotonically decreases with increasing θ, leading to the QME. By contrast, Type 2 states, which are degenerate in energy, have almost constant IPR values; this reflects in the almost-similar trace distance dynamics and the absence of the QME in the inset of Fig. 1(b).

QME in random Hamiltonians. To reveal the significance of energy distributions in the QME, we now construct a random model that allows us to tune the energy density and the IPR of an ensemble of initial states. We consider states in Eq. (2) with random angles on each site, i.e., θ_i, ϕ_i are independently drawn from the uniform distribution over a fraction f of its full domain. For a small f, the ensemble is close to a polarized state at a fixed energy, whereas $f = 1$ corresponds to an infinite temperature ensemble.

If the spins roughly all point in the same direction, any local term of the form $(\boldsymbol{\sigma}_i \times \boldsymbol{\sigma}_{i+1}) \cdot \hat{\mathbf{v}}$ has a zero expectation value, where $\hat{\mathbf{v}}$ is the unit vector along the three spin directions. In fact, the spectrum of this term is centered around zero, making all polarized states infinite temperature states for such Hamiltonians. To tune their energy density, we need to add terms that assign them a constant energy, e.g., an isotropic Heisenberg term of the form $\boldsymbol{\sigma}_i \cdot \boldsymbol{\sigma}_{i+1}$. Finally, a desired Hamiltonian is

$$H_R = \sum_{i=1}^{N-1} (\boldsymbol{\sigma}_i \times \boldsymbol{\sigma}_{i+1}) \cdot \hat{\mathbf{v}}_i + J_H \sum_i^{N-1} \boldsymbol{\sigma}_i \cdot \boldsymbol{\sigma}_{i+1}, \quad (7)$$

where the three components $\mathbf{v}_i = (v_x, v_y, v_z)_i$ are real numbers drawn uniformly from the window $[-1, 1]$ and we set $J_H = -4$. The random vectors $\hat{\mathbf{v}}_i$ ensure that the model breaks all global symmetries and it is nonintegrable, as confirmed by its average level spacing ratio matching the Wigner-Dyson prediction [65].

In Fig. 3(a) we show the overlaps of random states $|(\theta_i,\phi_i)\rangle$ with energy eigenstates of H_R, averaged over 100 realizations of the angles. For small f, the overlap peaks near the ground state, while in the limit $f \to 1$, the overlap is evenly distributed across the spectrum, moving the state toward infinite temperature. This coincides with a flattening of the distribution, as reflected in the decreasing IPR shown in the inset

of Fig. 3(b), marking delocalization over a larger number of eigenstates. Indeed, the QME is evident in the trace distance dynamics in Fig. 3(b), where increasing f leads simultaneously to higher initial $\Delta(\rho^A)$ values and faster decay rates, resulting in a crossing.

Floquet systems. Up to this point, we have focused on Hamiltonian systems with energy conservation. However, our previous considerations based on the IPR can be directly generalized to the Floquet eigenstates of a periodically driven system. To demonstrate the QME in the absence of energy conservation, we consider a Floquet version of Eq. (1), the kicked Ising model, with the Floquet operator given by [66–68]

$$U_{\mathrm{KI}} = \exp\left[-iT_1\left(J_{zz}\sum_j \sigma_j^z\sigma_{j+1}^z + h_z\sum_j \sigma_j^z\right)\right] \times \exp\left[-iT_2\ h_x\sum_j \sigma_j^x\right], \tag{8}$$

where we set the periods $T_1 = T_2 = 1/2$ for simplicity.

For $h_z \neq 0$, U_{KI} describes a chaotic model. Due to "Floquet heating" [69], for a generic initial condition, the state of the subsystem A then approaches the infinite-temperature thermal ensemble at late times, $\sigma^A = \mathbb{1}/\mathcal{D}_A$, where $\mathcal{D}_A$ is the Hilbert space dimension of A. This simplification in the Floquet case allows us to consider the relative entropy $S(\rho^A(t)||\sigma^A)$ [12] as a diagnostic of the QME, as the latter reduces to the entanglement entropy, $S_E = -\mathrm{Tr}\rho^A(t)\ln\rho^A(t)$, up to an unimportant constant factor involving $\mathcal{D}_A$.

For any pure and unentangled initial state, the initial relative entropy from σ^A is the same. Hence, to observe the QME in the Floquet case, we go beyond product states and consider weakly entangled initial states in the class of translation-invariant infinite matrix product states (iMPS) of the form $|\Psi(A)\rangle = \sum_{\mathbf{s}}(\cdots A^{[s_{i-1}]}A^{[s_i]}A^{[s_{i+1}]}\cdots)|\mathbf{s}\rangle$, where $|\mathbf{s}\rangle$ denotes the basis states [70]. For our purposes, it is sufficient to consider a single-parameter family of 2×2 MPS matrices A:

$$A^{[\downarrow]}(\theta) = \begin{pmatrix}\cos\theta & 0\\ \sin\theta & 0\end{pmatrix}, \quad A^{[\uparrow]}(\theta) = \begin{pmatrix}0 & -i\\ 0 & 0\end{pmatrix}. \tag{9}$$

This parametrization yields a normalized iMPS, and it has been used to describe quench dynamics in a constrained Ising model arising in Rydberg atom arrays [71,72].

Since entanglement growth is unbounded in an infinite Floquet system, the QME dynamics can be achieved if states with higher initial entanglement show a slower rate of entropy growth than states with smaller initial entanglement. To test this, we time evolve the states in Eq. (9) using the infinite time-evolving block decimation algorithm (iTEBD) [73] and evaluate the entanglement entropy dynamics for various values of θ in Fig. 4(a). With increasing θ, the initial entanglement in the state grows while its rate of growth simultaneously decreases, leading to multiple crossings in the S_E curves. This exemplifies the QME dynamics through the lens of entanglement entropy. To test the role of quasienergy distributions, we truncate the initial states to a finite chain of length N, and calculate their IPR in the Floquet eigenbasis in Fig. 4(b). The IPR behavior indeed correlates with the

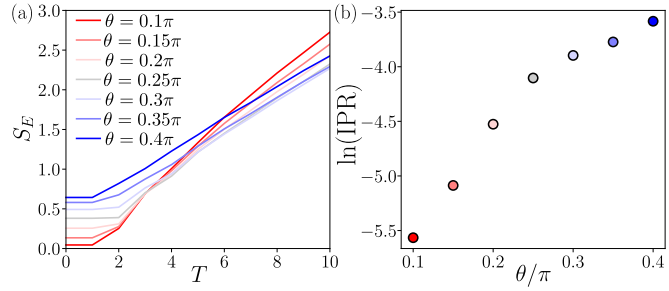

FIG. 4. QME in the kicked Ising model, Eq. (8). (a) Entanglement entropy dynamics of iMPS states (9) in integer multiples of the Floquet period $T = T_1 + T_2 = 1$ for several values of θ. The QME occurs as θ is increased. Data are obtained using iTEBD for the same parameters as specified below Eq. (1), and the bond dimension is $\chi = 128$. (b) Logarithm of IPR for a finite version of MPS states against the Floquet eigenstates obtained via exact diagonalization for the system size $N = 10$ with open boundary conditions.

crossings in entropy similar to previous results, e.g., Fig. 3(b) of the random model.

Conclusions. We demonstrated the ubiquity of the QME in a wide class of isolated quantum systems without special symmetries hitherto assumed. We elucidated a common origin of the QME based on energy distributions of initial states. This not only reproduces the earlier results for systems with global symmetries, but it also allows us to construct the QME in systems without such symmetries, including chaotic and random models. In the SM [59] we further demonstrate the generality of our conclusions by considering different choices of norms, initial states, and other measures. In particular, our findings show that previous observations of "strong" versus "weak thermalization" [74,75] in the same model can be now interpreted as an instance of the QME.

One interesting open question is: What is the universal diagnostic of the QME? In the SM [59], we confirm that simple spectral measures, such as energy variance and higher moments, generally do not account for our observations [59]. On the other hand, while the IPR is a good diagnostic for $|\theta,\phi\rangle$ product states as well as MPS states (9) considered above, the IPR diagnostic may break down for more highly entangled states. As a counterexample, it is enough to consider two initially low-entangled states that undergo time evolution *after* trace distance crossing. During subsequent evolution, they will no longer exhibit the QME; yet their IPR remains the same as it was at $t = 0$. We thus conjecture that, as a diagnostic of the QME, the IPR is limited to weakly entangled initial states. Formulating a precise general criterion remains an interesting open question.

Acknowledgments. We thank Andrew Hallam, Matthew Yusuf, Sara Murciano, and, in particular, Jie Ren for useful discussions. Some of the numerical simulations were performed using [76]. T.B. and Z.P. acknowledge support by the Leverhulme Trust Research Leadership Award No. RL-2019-015 and EPSRC Grant No. EP/Z533634/1. Work of L.S. and I.M., particularly on Floquet QME, was supported by the U.S. Department of Energy, Office of Science, Basic Energy Sciences, Materials Sciences and Engineering Division. A.A.C. acknowledges support from the Simons Foundation (Grant No. 669487). This research was supported in part by Grant

No. NSF PHY-2309135 to the Kavli Institute for Theoretical Physics (KITP).

Data availability. The data that support the findings of this article are openly available [77], embargo periods may apply.

[1] E. B. Mpemba and D. G. Osborne, Cool? Phys. Educ. **4**, 172 (1969).

[2] T. Keller, V. Torggler, S. B. Jäger, S. Schutz, H. Ritsch, and G. Morigi, Quenches across the self-organization transition in multimode cavities, New J. Phys. **20**, 025004 (2018).

[3] M. Baity-Jesi, E. Calore, A. Cruz, L. A. Fernandez, J. M. Gil-Narvión, A. Gordillo-Guerrero, D. Iñiguez, A. Lasanta, A. Maiorano, E. Marinari *et al.*, The Mpemba effect in spin glasses is a persistent memory effect, Proc. Natl. Acad. Sci. USA **116**, 15350 (2019).

[4] A. Kumar and J. Bechhoefer, Exponentially faster cooling in a colloidal system, Nature (London) **584**, 64 (2020).

[5] F. J. Schwarzendahl and H. Löwen, Anomalous cooling and overcooling of active colloids, Phys. Rev. Lett. **129**, 138002 (2022).

[6] I. G.-A. Pemartãn, E. Mompó, A. Lasanta, V. Martãn-Mayor, and J. Salas, Shortcuts of freely relaxing systems using equilibrium physical observables, Phys. Rev. Lett. **132**, 117102 (2024).

[7] H. C. Burridge and P. F. Linden, Questioning the Mpemba effect: Hot water does not cool more quickly than cold, Sci. Rep. **6**, 37665 (2016).

[8] I. Klich, O. Raz, O. Hirschberg, and M. Vucelja, Mpemba index and anomalous relaxation, Phys. Rev. X **9**, 021060 (2019).

[9] J. Bechhoefer, A. Kumar, and R. Chétrite, A fresh understanding of the Mpemba effect, Nat. Rev. Phys. **3**, 534 (2021).

[10] R. Holtzman and O. Raz, Landau theory for the Mpemba effect through phase transitions, Commun. Phys. **5**, 280 (2022).

[11] G. Teza, J. Bechhoefer, A. Lasanta, O. Raz, and M. Vucelja, Speedups in nonequilibrium thermal relaxation: Mpemba and related effects, arXiv:2502.01758.

[12] F. Ares, P. Calabrese, and S. Murciano, The quantum Mpemba effects, Nat. Rev. Phys. **7**, 451 (2025).

[13] F. Carollo, A. Lasanta, and I. Lesanovsky, Exponentially accelerated approach to stationarity in Markovian open quantum systems through the Mpemba effect, Phys. Rev. Lett. **127**, 060401 (2021).

[14] J. Zhang, G. Xia, C.-W. Wu, T. Chen, Q. Zhang, Y. Xie, W.-B. Su, W. Wu, C.-W. Qiu, P.-X. Chen *et al.*, Observation of quantum strong Mpemba effect, Nat. Commun. **16**, 301 (2025).

[15] S. Kochsiek, F. Carollo, and I. Lesanovsky, Accelerating the approach of dissipative quantum spin systems towards stationarity through global spin rotations, Phys. Rev. A **106**, 012207 (2022).

[16] R. Bao and Z. Hou, Accelerating relaxation in Markovian open quantum systems through quantum reset processes, arXiv:2212.11170.

[17] F. Ivander, N. Anto-Sztrikacs, and D. Segal, Hyperacceleration of quantum thermalization dynamics by bypassing long-lived coherences: An analytical treatment, Phys. Rev. E **108**, 014130 (2023).

[18] Y.-L. Zhou, X.-D. Yu, C.-W. Wu, X.-Q. Li, J. Zhang, W. Li, and P.-X. Chen, Accelerating relaxation through Liouvillian exceptional point, Phys. Rev. Res. **5**, 043036 (2023).

[19] A. K. Chatterjee, S. Takada, and H. Hayakawa, Quantum Mpemba effect in a quantum dot with reservoirs, Phys. Rev. Lett. **131**, 080402 (2023).

[20] A. K. Chatterjee, S. Takada, and H. Hayakawa, Multiple quantum Mpemba effect: Exceptional points and oscillations, Phys. Rev. A **110**, 022213 (2024).

[21] X. Wang and J. Wang, Mpemba effects in nonequilibrium open quantum systems, Phys. Rev. Res. **6**, 033330 (2024).

[22] D. Liu, J. Yuan, H. Ruan, Y. Xu, S. Luo, J. He, X. He, Y. Ma, and J. Wang, Speeding up quantum heat engines by the Mpemba effect, Phys. Rev. A **110**, 042218 (2024).

[23] S. Longhi, Photonic Mpemba effect, Opt. Lett. **49**, 5188 (2024).

[24] X. Wang, J. Su, and J. Wang, Mpemba meets quantum chaos: Anomalous relaxation and Mpemba crossings in dissipative Sachdev-Ye-Kitaev models, arXiv:2410.06669.

[25] J. Furtado and A. C. Santos, Strong quantum Mpemba effect with squeezed thermal reservoirs, Ann. Phys. **480**, 170135 (2025).

[26] D. Qian, H. Wang, and J. Wang, Intrinsic quantum Mpemba effect in Markovian systems and quantum circuits, Phys. Rev. B **111**, L220304 (2025).

[27] L. P. Bettmann and J. Goold, Information geometry approach to quantum stochastic thermodynamics, Phys. Rev. E **111**, 014133 (2025).

[28] J. W. Dong, H. F. Mu, M. Qin, and H. T. Cui, Quantum Mpemba effect of localization in the dissipative mosaic model, Phys. Rev. A **111**, 022215 (2025).

[29] A. Nava and R. Egger, Mpemba effects in open nonequilibrium quantum systems, Phys. Rev. Lett. **133**, 136302 (2024).

[30] I. Medina, O. Culhane, F. C. Binder, G. T. Landi, and J. Goold, Anomalous discharging of quantum batteries: The ergotropic Mpemba effect, Phys. Rev. Lett. **134**, 220402 (2025).

[31] F. Kheirandish, N. Cheraghpour, and A. Moradian, The Mpemba effect in quantum oscillating and two-level systems, Phys. Lett. A **559**, 130915 (2025).

[32] J. Graf, J. Splettstoesser, and J. Monsel, Role of electron-electron interaction in the Mpemba effect in quantum dots, J. Phys.: Condens. Matter **37**, 195302 (2025).

[33] K. Zatsarynna, A. Nava, R. Egger, and A. Zazunov, Green's function approach to Josephson dot dynamics and application to quantum Mpemba effects, Phys. Rev. B **111**, 104506 (2025).

[34] D. J. Strachan, A. Purkayastha, and S. R. Clark, Non-Markovian quantum Mpemba effect, arXiv:2402.05756.

[35] Z.-M. Wang, S. L. Wu, M. S. Byrd, and L.-A. Wu, Going beyond quantum Markovianity and back to reality: An exact master equation study, arXiv:2411.17197.

[36] P. Westhoff, S. Paeckel, and M. Moroder, Fast and direct preparation of a genuine lattice BEC via the quantum Mpemba effect, arXiv:2504.05549.

[37] S. Aharony Shapira, Y. Shapira, J. Markov, G. Teza, N. Akerman, O. Raz, and R. Ozeri, Inverse Mpemba effect demonstrated on a single trapped ion qubit, Phys. Rev. Lett. **133**, 010403 (2024).

[38] M. E. Edo and L.-A. Wu, Study on quantum thermalization from thermal initial states in a superconducting quantum computer, arXiv:2403.14630.

[39] J. M. Deutsch, Quantum statistical mechanics in a closed system, Phys. Rev. A **43**, 2046 (1991).

[40] M. Srednicki, Chaos and quantum thermalization, Phys. Rev. E **50**, 888 (1994).
[41] M. Rigol, V. Dunjko, and M. Olshanii, Thermalization and its mechanism for generic isolated quantum systems, Nature (London) **452**, 854 (2008).
[42] F. Ares, S. Murciano, and P. Calabrese, Entanglement asymmetry as a probe of symmetry breaking, Nat. Commun. **14**, 2036 (2023).
[43] S. Murciano, F. Ares, I. Klich, and P. Calabrese, Entanglement asymmetry and quantum Mpemba effect in the XY spin chain, J. Stat. Mech. (2024) 013103.
[44] C. Rylands, E. Vernier, and P. Calabrese, Dynamical symmetry restoration in the Heisenberg spin chain, J. Stat. Mech. (2024) 123102.
[45] S. Yamashika, F. Ares, and P. Calabrese, Entanglement asymmetry and quantum Mpemba effect in two-dimensional free-fermion systems, Phys. Rev. B **110**, 085126 (2024).
[46] S. Yamashika, P. Calabrese, and F. Ares, Quenching from superfluid to free bosons in two dimensions: Entanglement, symmetries, and quantum Mpemba effect, Phys. Rev. A **111**, 043304 (2025).
[47] X. Turkeshi, P. Calabrese, and A. D. Luca, Quantum Mpemba effect in random circuits, Phys. Rev. Lett. **135**, 040403 (2025).
[48] K. Klobas, C. Rylands, and B. Bertini, Translation symmetry restoration under random unitary dynamics, Phys. Rev. B **111**, L140304 (2025).
[49] S. Liu, H.-K. Zhang, S. Yin, and S.-X. Zhang, Symmetry restoration and quantum Mpemba effect in symmetric random circuits, Phys. Rev. Lett. **133**, 140405 (2024).
[50] H. Yu, Z.-X. Li, and S.-X. Zhang, Symmetry breaking dynamics in quantum many-body systems, arXiv:2501.13459.
[51] F. Ares, S. Murciano, P. Calabrese, and L. Piroli, Entanglement asymmetry dynamics in random quantum circuits, Phys. Rev. Res. **7**, 033135 (2025).
[52] K. Klobas, Non-equilibrium dynamics of symmetry-resolved entanglement and entanglement asymmetry: Exact asymptotics in Rule 54, J. Phys. A: Math. Theor. **57**, 505001 (2024).
[53] A. Foligno, P. Calabrese, and B. Bertini, Nonequilibrium dynamics of charged dual-unitary circuits, PRX Quantum **6**, 010324 (2025).
[54] S. Liu, H.-K. Zhang, S. Yin, S.-X. Zhang, and H. Yao, Quantum Mpemba effects in many-body localization systems, arXiv:2408.07750.
[55] L. K. Joshi, J. Franke, A. Rath, F. Ares, S. Murciano, F. Kranzl, R. Blatt, P. Zoller, B. Vermersch, P. Calabrese *et al.*, Observing the quantum Mpemba effect in quantum simulations, Phys. Rev. Lett. **133**, 010402 (2024).
[56] C. Rylands, K. Klobas, F. Ares, P. Calabrese, S. Murciano, and B. Bertini, Microscopic origin of the quantum Mpemba effect in integrable systems, Phys. Rev. Lett. **133**, 010401 (2024).
[57] P. Calabrese and J. Cardy, Evolution of entanglement entropy in one-dimensional systems, J. Stat. Mech. (2005) P04010.
[58] H. Kim and D. A. Huse, Ballistic spreading of entanglement in a diffusive nonintegrable system, Phys. Rev. Lett. **111**, 127205 (2013).
[59] See Supplemental Material at http://link.aps.org/supplemental/10.1103/1td3-2vwf for additional numerical results and study of other models.
[60] L. D'Alessio, Y. Kafri, A. Polkovnikov, and M. Rigol, From quantum chaos and eigenstate thermalization to statistical mechanics and thermodynamics, Adv. Phys. **65**, 239 (2016).
[61] A. Russotto, F. Ares, and P. Calabrese, Symmetry breaking in chaotic many-body quantum systems at finite temperature, Phys. Rev. E **112**, L032101 (2025).
[62] F. Ares, V. Vitale, and S. Murciano, Quantum Mpemba effect in free-fermionic mixed states, Phys. Rev. B **111**, 104312 (2025).
[63] F. Caceffo, S. Murciano, and V. Alba, Entangled multiplets, asymmetry, and quantum Mpemba effect in dissipative systems, J. Stat. Mech. (2024) 063103.
[64] D. J. Thouless, Electrons in disordered systems and the theory of localization, Phys. Rep. **13**, 93 (1974).
[65] V. Oganesyan and D. A. Huse, Localization of interacting fermions at high temperature, Phys. Rev. B **75**, 155111 (2007).
[66] T. Prosen, Time evolution of a quantum many-body system: Transition from integrability to ergodicity in the thermodynamic limit, Phys. Rev. Lett. **80**, 1808 (1998).
[67] T. Prosen, Quantum invariants of motion in a generic many-body system, J. Phys. A: Math. Gen. **31**, L645 (1998).
[68] B. Bertini, P. Kos, and T. Prosen, Entanglement spreading in a minimal model of maximal many-body quantum chaos, Phys. Rev. X **9**, 021033 (2019).
[69] M. Bukov, L. D'Alessio, and A. Polkovnikov, Universal high-frequency behavior of periodically driven systems: from dynamical stabilization to Floquet engineering, Adv. Phys. **64**, 139 (2015).
[70] J. I. Cirac, D. Pérez-García, N. Schuch, and F. Verstraete, Matrix product states and projected entangled pair states: Concepts, symmetries, theorems, Rev. Mod. Phys. **93**, 045003 (2021).
[71] W. W. Ho, S. Choi, H. Pichler, and M. D. Lukin, Periodic orbits, entanglement, and quantum many-body scars in constrained models: Matrix product state approach, Phys. Rev. Lett. **122**, 040603 (2019).
[72] A. Daniel, A. Hallam, J.-Y. Desaules, A. Hudomal, G.-X. Su, J. C. Halimeh, and Z. Papić, Bridging quantum criticality via many-body scarring, Phys. Rev. B **107**, 235108 (2023).
[73] G. Vidal, Classical simulation of infinite-size quantum lattice systems in one spatial dimension, Phys. Rev. Lett. **98**, 070201 (2007).
[74] M. C. Bañuls, J. I. Cirac, and M. B. Hastings, Strong and weak thermalization of infinite nonintegrable quantum systems, Phys. Rev. Lett. **106**, 050405 (2011).
[75] C.-J. Lin and O. I. Motrunich, Quasiparticle explanation of the weak-thermalization regime under quench in a nonintegrable quantum spin chain, Phys. Rev. A **95**, 023621 (2017).
[76] J. Ren, iTEBD.jl, https://github.com/jayren3996/iTEBD.jl.
[77] Data repository this paper, https://doi.org/10.5518/1741.